Journal of Sound and Vibration 387 (2017) 114–126

Contents lists available at ScienceDirect

Journal of Sound and Vibration

journal homepage: www.elsevier.com/locate/jsvi

Vibroacoustic modeling of an acoustic resonator tuned by dielectric elastomer membrane with voltage control

Xiang Yu [a], Zhenbo Lu [b], Li Cheng [c], Fangsen Cui [a,*]

[a] Institute of High Performance Computing, A*STAR, Singapore 138632, Singapore
[b] Temasek Laboratories, National University of Singapore, Singapore 117411, Singapore
[c] Department of Mechanical Engineering, The Hong Kong Polytechnic University, 999011 Hong Kong

ARTICLE INFO

Article history:
Received 29 December 2015
Received in revised form
28 August 2016
Accepted 13 October 2016
Handling Editor: L.G. Tham
Available online 22 October 2016

Keywords:
Acoustic resonator
Dielectric elastomer
Membrane silencer
Adaptive-passive control
Vibroacoustic modeling

ABSTRACT

This paper investigates the acoustic properties of a duct resonator tuned by an electro-active membrane. The resonator takes the form of a side-branch cavity which is attached to a rigid duct and covered by a pre-stretched Dielectric Elastomer (DE) in the neck area. A three-dimensional, analytical model based on the sub-structuring approach is developed to characterize the complex structure-acoustic coupling between the DE membrane and its surrounding acoustic media. We show that such resonator provides sound attenuation in the medium frequency range mainly by means of sound reflection, as a result of the membrane vibration. The prediction accuracy of the proposed model is validated against experimental test. The pre-stretched DE membrane with fixed edges responds to applied voltage change with a varying inner stress and, by the same token, its natural frequency and vibrational response can be tuned to suit particular frequencies of interest. The peaks in the transmission loss (TL) curves can be shifted towards lower frequencies when the voltage applied to the DE membrane is increased. Through simulations on the effect of increasing the voltage level, the TL shifting mechanism and its possible tuning range are analyzed. This paves the way for applying such resonator device for adaptive-passive noise control.

1. Introduction

Design of acoustic resonators for sound control inside ducts is an important topic for industrial applications. Passive devices such as Helmholtz resonators and quarter-wave tubes have been extensively investigated and implemented [1]. The geometry and the component of a passive resonator are usually fixed for the purpose of structural simplicity and easy maintenance, which however limits its acoustic performance to single or very narrow frequency band. Adaptive or tunable devices with adjustable physical parameters offer an attractive alternative. For example, Zhao and Morgans [2] proposed a Helmholtz resonator design to control the combustion instabilities, where neck area of the resonator can be altered to provide damping effect for multiple unstable modes at different frequencies. Nagaya et al. [3] presented a two-stage Helmholtz resonator with auto-tuning mechanism to control the noise peaks of a blower. Howard and Craig [4] developed an adaptive quarter-wave tube with a variable length to tune the effective TL position, and assessed its effectiveness as a petrol engine silencer.

* Corresponding author.
E-mail address: cuifs@ihpc.a-star.edu.sg (F. Cui).

http://dx.doi.org/10.1016/j.jsv.2016.10.022
0022-460X/

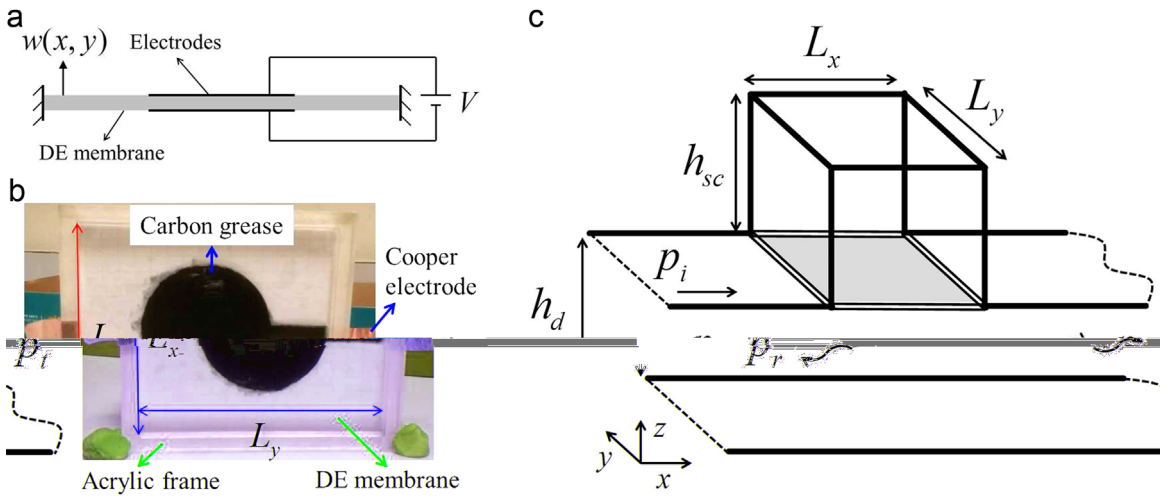

Fig. 1. a) Cross-section of a DE membrane, pre-stretched and fixed onto a rigid frame. b) Fabricated sample of a pre-stretched DE membrane coated with electrodes. (c) A tunable acoustic resonator being attached to a rigid duct. The opening at the neck area is covered by a DE membrane.

Introducing smart materials to acoustic systems offers some potential applications for designing adaptive devices [5]. Among the existing categories of electro-active polymers, dielectric elastomer (DE) shows promising features such as low-cost, lightweight, and fast response to electrical field [6]. The electrical-mechanical coupling between DE and the applied electrical field have been extensively investigated [7,8]. As shown in Fig. 1(a) & (b), a typical DE film takes the form of a pre-stretched membrane fixed onto a rigid frame, where compliant electrodes are coated on both sides of the membrane surface for applying voltage. Technologies such as metal sputtering process [9] and ion implantation [10] have been developed to fabricate lightweight electrodes, which well maintains the flexibility of the DE film. When a sufficiently high voltage is applied, the electric force squeezes the DE membrane between the electrodes and causes an in-plane elongation in the surface. Consequently, an increasing applied voltage level results in a decrease in the membrane internal stress [10]. Although a number of studies in the literature have analyzed the resonance frequency shift and large deformation behavior of the membrane itself [6,7,9–11], the use of dielectric elastomer for acoustic applications has been fairly limited, except for only a few reports on using DE as loudspeakers [9,12,13].

Recently, Lu et al. [14] demonstrated experimentally that, the use of a DE membrane with voltage control can actively tune the TL characteristics of an acoustic resonator. The basic configuration of the system is shown in Fig. 1(c), where a rectangular side-branch resonator is attached to a rigid duct, with its opening at the neck area covered by a DE membrane. The duct has a height of h_d and the pre-stretched membrane being mounted onto the rigid frame has a cross-section area of $L_x \times L_y$. The height of the backing side-branch cavity is h_{sc}. Inside the rigid duct, the incoming sound wave p_i is scattered by the resonator into the reflected (p_r) and transmitted (p_t) sound waves, leading to a reduction in the transmitted sound power as a result of the destructive acoustic interference. Therefore, an effective sound attenuation of such device requires a strong membrane vibration and an efficient sound radiation back to duct upstream.

Physically speaking, the system shown in Fig. 1(c) involves the complex structure-acoustic coupling between acoustic fields inside the duct and side-branch cavity, as a result of the induced membrane vibration. This resembles the passive drum silencer configuration proposed by Huang *et al.* for low-frequency sound attenuation, which has received careful and systematic investigations [15–19]. Among Huang's studies, a modal analysis was originally conducted on a two-dimensional system [16] to reveal the detailed modal coupling mechanism, and later a three-dimensional formulation [19] was presented to address the counterproductive effect of membrane lateral tension. It is, however, worthy noting that the present configuration differs from Huang's system in two aspects. First, Huang's silencer is characterized by a high aspect ratio ($L_x/L_y = 5$) such that the membrane response is highly one-dimensional, essentially like a string. Second, the membrane material and the tension force cannot be adjusted once the silencer is designed. The proposed acoustic resonator, in contrast, has an aspect ratio close to unity, and the utilized DE membrane can be actively tuned with a varying voltage to produce the desired inner stress and natural frequency. This further changes the coupled response of the vibrating membrane and thus the silencing performance provided by the resonator.

In terms of numerical modeling, Huang *et al.* [15–19] used a mode-matching method to couple the acoustic fields on both sides of the membrane. A more rigorous mathematical formulation was later supplemented by Lawrie and Guled [20]. The mode-matching method involves extensive integrations over the boundaries to couple different modal spaces; further extension to more complex configuration may quickly become cumbersome. Alternatively, finite element method (FEM) can be used [21]. With FEM, non-linear effects such as large membrane deformation or buckling could be considered. However, FEM simulation for such structure-acoustic interaction problem can be highly computational demanding, which in turn limits its ability in performing a systematic parametric analysis and optimization study.

Based on the above discussions, this paper aims at developing a three-dimensional, fully coupled vibroacoustic model to

facilitate the prediction, analysis and design of the acoustic resonator incorporating tunable DE membranes. To this end, a sub-structuring formulation [22,23] is implemented, which solves the structure-acoustic interactions by assembling the subsystem transfer functions predetermined at the coupling interfaces. The modeling framework is inspired by the Patch Transfer Function (PTF) approach proposed by Ouisse et al. [24,25]. These transfer functions are calculated on averaged patches in order to reduce the numbers of degrees of freedom (n-DOF) involved in each subsystem, and to enable a convenient interface matching treatment. The subsystem modules for constructing the configuration shown in Fig. 1(c), which are in regular geometries allowing standard Fourier series formulations, are developed based on modal expansion approach to save the computational cost.

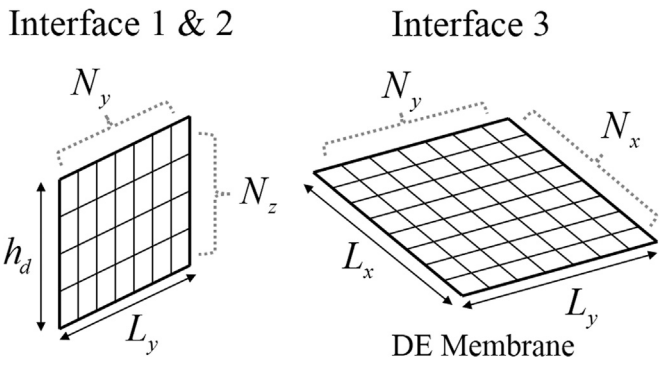

Fig. 3. Division of patches at the three interfaces.

1 and 2 with a cross-section area of $L_y \times h_d$ are segmented into $N_y \times N_z$ patches, and the interface 3 with a cross-section area of $L_x \times L_y$ has $N_x \times N_y$ patches. By doing so, the force and velocity vectors for describing the k-th interface with a total number of N patches are written as:

$$\mathbf{F}_k = \left[F_{k1};\ F_{k2};\ \cdots F_{kN}\right];\quad \mathbf{U}_k = \left[U_{k1};\ U_{k2};\ \cdots U_{kN}\right] \qquad k = 1,\ 2,\ 3 \tag{1}$$

According to Fig. 2(b), the DE membrane at interface 3 vibrates under a given excitation force, which can be described by:

$$\mathbf{U}_3 = \mathbf{Y}_m\mathbf{F}_3 = \begin{bmatrix} Y_{11} & \cdots & Y_{1N} \\ \vdots & \ddots & \vdots \\ Y_{N1} & \cdots & Y_{NN} \end{bmatrix}\begin{bmatrix} F_1 \\ \vdots \\ F_N \end{bmatrix} = \begin{bmatrix} U_1 \\ \vdots \\ U_N \end{bmatrix}, \tag{2}$$

where $\mathbf{U}_3$ is the vector of normal vibrating velocity of the membrane; $\mathbf{F}_3$ is the excitation force vector with each element $F_N = \Delta p \times \Delta s$, where Δp is the pressure difference acting on the membrane at each patch and Δs is the patch surface area; $\mathbf{Y}_m$ is referred to as the mobility of the DE membrane, whose expression will be derived in Section 2.2.

At interfaces 1 and 2, the incident sound wave introduces an exciting force $\mathbf{F}_i$ to the system, and the reflected and transmitted sound waves are described using a semi-infinite duct radiation model. The coupling forces through the acoustic cavity between the inlet and outlet ducts are first denoted as $\mathbf{F}_1^c$ and $\mathbf{F}_2^c$. Continuity of pressure (force) and normal velocity gives:

$$\begin{aligned} \mathbf{F}_i - \mathbf{Z}_d\mathbf{U}_1 &= \mathbf{F}_1^c \\ \mathbf{F}_2^c &= \mathbf{Z}_d\mathbf{U}_2 \end{aligned}, \tag{3}$$

where $\mathbf{U}_1$ and $\mathbf{U}_2$ are the normal velocities of interface 1 and 2. $\mathbf{Z}_d$ is the acoustic radiation impedance of a semi-infinite duct, so that the radiation loading force can be calculated as $\mathbf{F}_d = \mathbf{Z}_d\mathbf{U}_d$. The DE membrane at interface 3 vibrates under the acoustic excitation force and acoustic loading exerted on its bottom and top surfaces:

$$\mathbf{Y}_m(\mathbf{F}_3^c - \mathbf{Z}_{sc}\mathbf{U}_3) = \mathbf{U}_3, \tag{4}$$

where $\mathbf{U}_3$ is the vibrating velocity of interface 3; $\mathbf{F}_3^c$ is the acoustic excitation from the main duct; $\mathbf{Z}_{sc}\mathbf{U}_3$ is the acoustic loading from the side-branch cavity, with $\mathbf{Z}_{sc}$ being the cavity impedance.

The coupling forces $\mathbf{F}_1^c$, $\mathbf{F}_2^c$, $\mathbf{F}_3^c$ acting on the boundaries of the cavity in Fig. 2(b), induced by the vibrating boundary velocities themselves, can be expressed as:

$$\begin{aligned} \mathbf{F}_1^c &= \mathbf{Z}_{11}^c\mathbf{U}_1 + \mathbf{Z}_{12}^c\mathbf{U}_2 + \mathbf{Z}_{13}^c\mathbf{U}_3 \\ \mathbf{F}_2^c &= \mathbf{Z}_{21}^c\mathbf{U}_1 + \mathbf{Z}_{22}^c\mathbf{U}_2 + \mathbf{Z}_{23}^c\mathbf{U}_3, \\ \mathbf{F}_3^c &= \mathbf{Z}_{31}^c\mathbf{U}_1 + \mathbf{Z}_{32}^c\mathbf{U}_2 + \mathbf{Z}_{33}^c\mathbf{U}_3 \end{aligned} \tag{5}$$

or, in a compact matrix form as:

$$\begin{bmatrix} \mathbf{F}_1^c \\ \mathbf{F}_2^c \\ \mathbf{F}_3^c \end{bmatrix} = \begin{bmatrix} \mathbf{Z}_{11}^c & \mathbf{Z}_{12}^c & \mathbf{Z}_{13}^c \\ \mathbf{Z}_{21}^c & \mathbf{Z}_{22}^c & \mathbf{Z}_{23}^c \\ \mathbf{Z}_{31}^c & \mathbf{Z}_{32}^c & \mathbf{Z}_{33}^c \end{bmatrix}\begin{bmatrix} \mathbf{U}_1 \\ \mathbf{U}_2 \\ \mathbf{U}_3 \end{bmatrix}, \tag{6}$$

where $\mathbf{Z}_c = \left[\mathbf{Z}_{11}^c, \mathbf{Z}_{12}^c, \mathbf{Z}_{13}^c;\ \mathbf{Z}_{21}^c, \mathbf{Z}_{22}^c, \mathbf{Z}_{23}^c;\ \mathbf{Z}_{31}^c, \mathbf{Z}_{32}^c, \mathbf{Z}_{33}^c\right]$ are the acoustic impedances between the corresponding interfaces of the rectangular acoustic cavity.

By substituting Eq. (5) into Eqs. (3) and (4), the coupled system response can be solved by numerically inversing the following matrix:

$$\begin{bmatrix} \mathbf{Z}_{11}^c + \mathbf{Z}_d & \mathbf{Z}_{12}^c & \mathbf{Z}_{13}^c \\ \mathbf{Z}_{21}^c & \mathbf{Z}_{22}^c - \mathbf{Z}_d & \mathbf{Z}_{23}^c \\ \mathbf{Y}_m\mathbf{Z}_{31}^c & \mathbf{Y}_m\mathbf{Z}_{32}^c & \mathbf{Y}_m(\mathbf{Z}_{33}^c - \mathbf{Z}_{sc}) - \mathbf{I} \end{bmatrix} \begin{bmatrix} \mathbf{U}_1 \\ \mathbf{U}_2 \\ \mathbf{U}_3 \end{bmatrix} = \begin{bmatrix} \mathbf{F}_i \\ \mathbf{0} \\ \mathbf{0} \end{bmatrix}, \tag{7}$$

where $\mathbf{I}$ is an identity matrix whose size equals to the number of divided patches at interface 3.

As depicted in Fig. 2(a), the principle of energy conservation requires that the power being injected to the system equals to the power being reflected, transmitted and dissipated. The injected power Π_1^i corresponding to a plane wave excitation with pressure amplitude p_i is:

$$\Pi_1^i = |p_i|^2 S_1/(2\rho_0 c_0), \tag{8}$$

where S_1 is the surface area of interface 1. The air density ρ_0 is taken as 1.213 kg/m^3, and sound speed in air c_0 = 340 m/s. At interface 2, the transmitted power to the downstream of the duct is calculated as:

$$\Pi_2^t = \int_{S_2} \frac{1}{2}(p_t \times U_2^*)dS_2 = \frac{1}{2}(\mathbf{F}_2^c)\cdot(\mathbf{U}_2^*) = \frac{1}{2}(\mathbf{Z}_d\mathbf{U}_2)\cdot(\mathbf{U}_2^*), \tag{9}$$

where S_2 is the surface area of interface 2; the asterisk denotes the complex conjugate of the velocity. The TL of the system is then:

$$\mathrm{TL} = 10\ \log(\Pi_1^i/\Pi_2^t). \tag{10}$$

Similarly, the sound power transmitted into the cavity between the inlet and outlet ducts, from interface 1, is:

$$\Pi_1^t = \frac{1}{2}(\mathbf{F}_1^c)\cdot(\mathbf{U}_1^*) = \frac{1}{2}(\mathbf{F}_i - \mathbf{Z}_d\mathbf{U}_1)\cdot(\mathbf{U}_1^*). \tag{11}$$

The reflected power Π_1^r back to the upstream from interface 1, and the absorbed power Π^α by the resonator between interface 1 and 2, are then:

$$\begin{aligned} \Pi_1^r &= \Pi_1^i - \Pi_1^t \\ \Pi^\alpha &= \Pi_1^t - \Pi_2^t \end{aligned} \tag{12}$$

After the reflected and absorbed sound powers have been separated, the reflection and absorption coefficients of the system, i.e., R and α, can be calculated as:

$$\begin{aligned} R &= \Pi_1^r/\Pi_1^i = 1 - \Pi_1^t/\Pi_1^i \\ \alpha &= (\Pi_1^t - \Pi_2^t)/\Pi_1^i \end{aligned} \tag{13}$$

This forms a complete description and characterization of the system by determining the velocity responses at the interfaces, the system TL and the relative strength of sound reflection and absorption. The detailed subsystem treatments constituting the remaining modeling work are demonstrated in the following subsections.

2.2. Membrane modeling

Analytical modeling of the two-dimensional DE membrane is presented. As shown in Fig. 1, a rectangular, pre-stretched membrane is fixed along the four edges, covering the opening between the main duct and side-branch cavity with a cross-section area of $L_x \times L_y$. The initial, stress-free state of the elastomer has a side length of L_x^0 and L_y^0, so that the pre-stretch ratios in the x and y directions are defined as:

$$\delta_x = L_x/L_x^0; \quad \delta_y = L_y/L_y^0. \tag{14}$$

Here, for the sake of simplicity, the experiment [14] and the following theoretical analyses consider an identical pre-stretch ratio, i.e., $\delta = \delta_x = \delta_y$. Assuming a constant total volume of the DE membrane, the thickness of the membrane in the stretched state t_m is:

$$t_m = t_m^0/\delta^2, \tag{15}$$

where t_m^0 is the elastomer thickness in the initial state before stretching. The distributed tensile force per unit length being applied to the pre-stretched membrane in both the axial and lateral directions is:

$$T = \sigma t_m, \tag{16}$$

where σ is the inner stress of the membrane in the x and y plane.

Assuming that no buckling or bending occurs when an actuation voltage V is applied, the electrostatic force results in a decrease in the membrane stress, whose relation is theoretically characterized by [9,10]:

$$\sigma' = \sigma - \varepsilon V^2/t_m, \tag{17}$$

where σ' is the altered membrane stress due to the introduced voltage control; ε is the permittivity of the elastomer.

When a harmonic excitation of pressure difference $\Delta p e^{j\omega t}$ is added onto the membrane, its flexural vibration is governed by:

$$T\nabla^2 w(x, y, t) + \omega^2 \rho_m t_m w(x, y, t) = -\Delta p e^{j\omega t}, \tag{18}$$

where $w(x, y, t)$ is the membrane displacement in the z direction; T is the tensile force in Eq. (16); ρ_m is the DE material density; $c_m = \sqrt{T/\rho_m t_m}$. The damping effect can be accounted by using a complex angular frequency $\omega^* = \omega/\sqrt{1 + j\eta_m}$, where η_m is the equivalent damping loss factor of the membrane.

On omitting the time dependent term $e^{j\omega t}$ and using the modal expansion approach, the membrane displacement can be expressed as a summation of the *in-vacuo* structural modes as:

$$w(x, y) = \sum_n a_n \Phi_n(x, y), \tag{19}$$

where a_n is the modal amplitude of the n-th eigenmode and $\Phi_n(x, y)$ is the corresponding mode shape function. The expression of $\Phi_n(x, y)$ satisfying the fixed boundary conditions is given by [19]:

$$\Phi_n(x, y) = \sin\left(\frac{n_x \pi}{L_x} x\right) \sin\left(\frac{n_y \pi}{L_y} y\right), \quad n_x = n_y = 1, 2, 3\cdots, \tag{20}$$

where n_x and n_x are the modal indices in the x and y directions, respectively.

The mobility of the DE membrane in Eq. (2) is obtained by deriving the transfer function between the exciting patch and receiving patch. Given an averaged excitation force $\overline{F_q} = \overline{\Delta p}(x_q, y_q) \times \Delta s$ at an exciting patch q, where $\overline{\Delta p}$ is the averaged pressure difference provided that the patch size is sufficiently small, on substituting Eq. (19) into Eq. (18) and making use of the modal orthogonality property, the membrane response can be calculated as:

$$a_n(\omega_n^2 - \omega^2) M_n = \int_s \frac{\overline{F_q}}{\Delta s} \Phi_n dS_q, \tag{21}$$

where ω_n and M_n are the natural frequencies and modal masses of the membrane, given by:

$$\omega_n = \pi c_m \sqrt{\left(\frac{n_x}{L_x}\right)^2 + \left(\frac{n_y}{L_y}\right)^2}$$
$$M_n = \rho_m t_m \int_s \Phi_n^2 dS = \frac{\rho_m t_m L_x L_y}{4} \tag{22}$$

The velocity response for the points located within a receiving patch p is:

$$U_p(x_p, y_p) = \sum_n j\omega a_n \Phi_n(x_p, y_p) = \sum_n \frac{j\omega \Phi_n(x_p, y_p)}{(\omega_n^2 - \omega^2) M_n \Delta s} \int_s \overline{F_q} \Phi_n dS_q, \tag{23}$$

and a surface average $\overline{U_p} = \int_s U_p(x_p, y_p) dS_p/\Delta s$ can be used to account for the effective patch velocity. The transfer function Y_m between the averaged force $\overline{F_q}$ and averaged velocity $\overline{U_p}$ yields:

$$Y_m = \frac{\overline{U_p}}{\overline{F_q}} = \sum_n \frac{j\omega}{(\omega_n^2 - \omega^2) M_n \Delta s^2} \int_s \Phi_n dS_p \int_s \Phi_n dS_q. \tag{24}$$

Numerically, the above equation is truncated with a sufficient number of structural modes. Denoting the integration of eigenfunction Φ_n over the N-th patch as $X_N = \int_s \Phi_n dS_N$ so that a column vector $\mathbf{X} = [X_1, X_2, \cdots X_N]$, the membrane mobility $\mathbf{Y}_m$ in Eq. (2) eventually becomes:

$$\mathbf{Y}_m = \sum_n \beta_n \mathbf{X} \otimes \mathbf{X} = \sum_n \beta_n \begin{bmatrix} X_1X_1 & \cdots & X_1X_N \\ \vdots & \ddots & \vdots \\ X_NX_1 & \cdots & X_NX_N \end{bmatrix}, \tag{25}$$

where $\beta_n = j\omega/[(\omega_n^2 - \omega^2) M_n \Delta s^2]$.

2.3. Cavity and duct modeling

The formulation procedures for the two acoustic cavities and semi-infinite radiation ducts are briefly presented. Consider the three-dimensional acoustic cavities below and above the DE membrane, the sound pressure field can be expressed as an expansion of the acoustic eigenmodes as:

$$p(x, y, z) = \sum_r a_r \varphi_r(x, y, z), \tag{26}$$

where a_r is the modal amplitude of the r-th mode and φ_r is the acoustic mode shape function.

Using Green's identity to account for the cavity boundary conditions gives:

$$\int_{V_c} (p\nabla^2\varphi_r - \varphi_r \nabla^2 p) dV_c = \int_{S_c} \left(p\frac{\partial \varphi_r}{\partial n} - \varphi_r \frac{\partial p}{\partial n} \right) dS_c, \tag{27}$$

where V_c and S_c are the volume and boundary surface of the cavity.

For the rectangular cavities shown in Fig. 2(a), rigid-walled acoustic modes with standard Fourier cosine series can be assumed to calculate the induced sound pressure field by a vibrating boundary. Consider a boundary segment is vibrating with an averaged velocity $\overline{U_q}$, the Helmholtz equation and boundary conditions are:

$$\begin{aligned} &\nabla^2 p + k^2 p = 0; \quad \partial p/\partial n = -j\rho_0 \omega \overline{U_q} \\ &\nabla^2 \varphi_r + k_r^2 \varphi_r = 0; \quad \partial \varphi_r/\partial n = 0 \end{aligned}, \tag{28}$$

where $k_r = \omega_r/c_0 = 2\pi f_r/c_0$, f_r is the cavity natural frequency.

Substituting Eq. (28) into Eq. (27) yields the modal response of the cavity:

$$a_r N_r (k^2 - k_r^2) = j\rho_0 \omega \int_s \overline{U_q} \varphi_r dS_q, \tag{29}$$

where $N_r = \int_{V_c} \varphi_r \varphi_r' dV_c$.

The cavity impedance Z_c is defined as the transfer function between averaged velocity $\overline{U_p}$ and averaged force $\overline{F_q}$ as:

$$Z_c = \frac{\overline{F_q}}{\overline{U_p}} = \sum_r \frac{j\rho_0 \omega}{N_r (k^2 - k_r^2)} \int_s \varphi_r dS_p \int_s \varphi_r dS_q. \tag{30}$$

Similar to Eq. (25), the above equation is truncated numerically with a sufficient number of acoustic modes to calculate the impedance matrices $\mathbf{Z}_c$ and $\mathbf{Z}_{sc}$ for the two cavities below and above the membrane, respectively.

As to the two semi-infinite ducts constituting the inlet and outlet domain, sound radiation is constrained by the rigid duct walls and the sound pressure can be expressed as:

$$p(x, y, z) = \sum_s a_s \psi_s(y, z) e^{-jk_x x}, \tag{31}$$

where a_s and ψ_s are the modal amplitude and planner eigenfunction in the rectangular duct cross-section. x is the direction for radiated waves, with positive being away from the duct end. The corresponding wavenumber is $k_x = \sqrt{(\omega/c_0)^2 - k_s^2}$. When an exciting patch q is vibrating at the duct end (x=0) with an averaged normal velocity $\overline{U_q}$,

$$\partial p/\partial x = \sum_s -jk_x a_s \psi_s(y, z) = -j\rho_0 \omega \overline{U_q}. \tag{32}$$

Multiplying the above equation by ψ_s and integrating over the cross-section area, the model amplitude is calculated as:

$$a_s = \frac{\rho_0 \omega}{k_x N_s} \int_s \overline{U_q} \psi_s dS_q, \tag{33}$$

where $N_s = \int_s \psi_s \psi_s' dS$. The duct radiation impedance eventually becomes:

$$Z_d = \frac{\overline{F_q}}{\overline{U_p}} = \sum_s \frac{\rho_0 \omega}{N_s k_x} \int_s \psi_s dS_p \int_s \psi_s dS_q. \tag{34}$$

The cavity and duct impedances determined by Eqs. (30) and (34), together with the membrane mobility by Eq. (24), are assembled in Eq. (7) to solve the ensemble response of the resonator system. It is worth mentioning that the proposed modal formulation allows the use of both standard trigonometric series and the numerical outputs (e.g., from FEM) as the subsystem eigenfunctions. The analyses in this article adopt the former analytical roots for describing regular-shaped subsystems in Fig. 2(a). Nevertheless, the effects of electrodes' mass (either uniformly or non-uniformly distributed on the membrane), irregular shaped subsystems, or large/non-linear membrane deformation can be taken into account by using numerical solutions.

3. Validation

Before employing the developed numerical model to study the acoustic performance of the proposed resonator with voltage control, a model validation was carried out first. The first case considers the drum silencer configuration proposed by

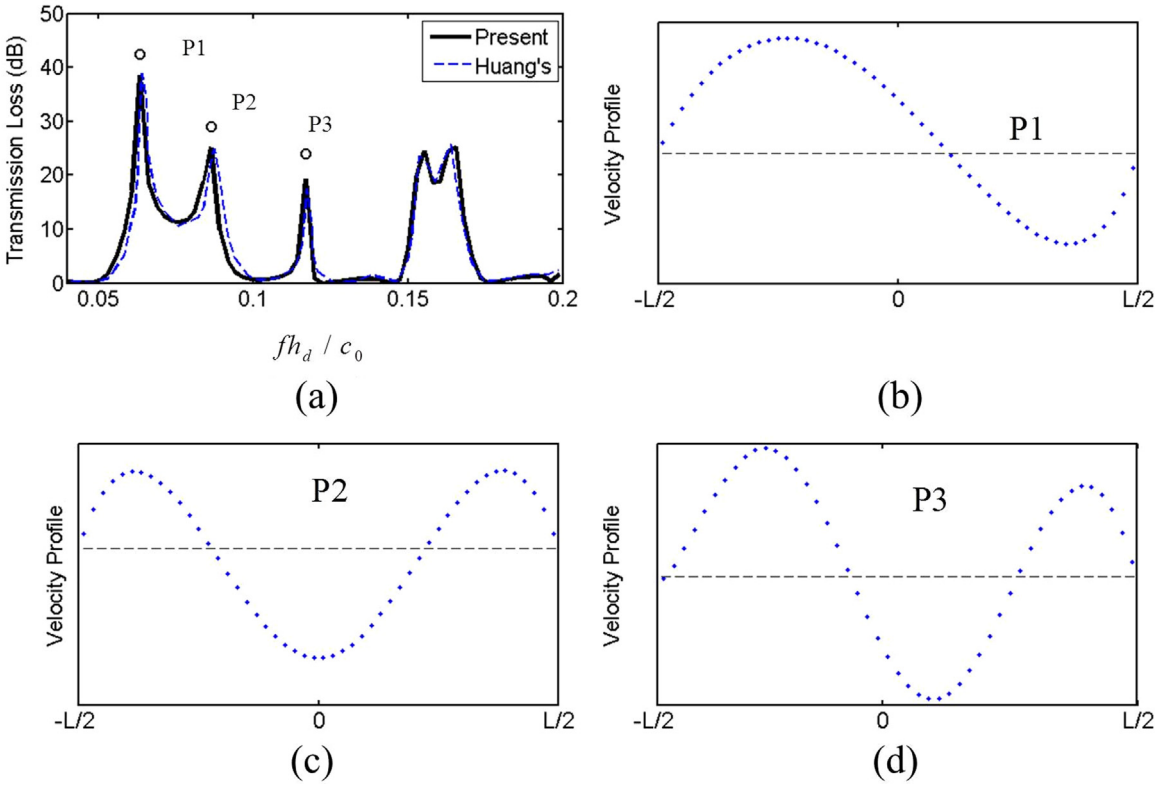

Fig. 4. (a) Transmission loss of the drum silencer, in agreement with Ref. [19]; (b) The membrane responses at the three distinct peaks, P1 = 0.0625; (c) P2 = 0.085; (d) P3 = 0.117.

Huang et al. [15–19], which deals with an expansion chamber with high aspect ratio and an aluminum membrane under high tension. The parameters input to the simulation model are the same as those used in Huang's three-dimensional study [19]. The non-dimensional variables given by Huang and Choy [19] are reverted to dimensional ones as:

$$\begin{aligned} &h_d = h_{sc} = L_y = 0.17\text{m}; && L_x = 5L_y = 0.85\ \text{m}; \\ &\rho_{\text{m}} = 2700\ \text{kg}/m^3; && t_{\text{m}} = 0.000077\ \ m = 0.077\text{mm} \\ &T_x = 0.475\rho_0(c_0 h_d)^2 = 1900\ \text{N}/m; && T_y = 0.08T_x \end{aligned} \tag{35}$$

where T_x and T_y are the tensile forces in the x and y directions, respectively.

The dimensional frequency range of interest is chosen from 50 to 400 Hz, corresponding to a non-dimensional frequency (defined as fh_d/c_0) from 0.025 to 0.2. In the simulation, the modal truncation was enabled by an automatic algorithm to include enough structural and acoustic modes. The segmentation of patches in Fig. 3 was made in accordance with the embedded wavelength of interest to ensure a valid assumption of the averaged force and velocity. Here, a criterion of $\Delta l = c/2f_c$ as proposed by Ouisse et al. [25] was adopted, with Δl being the allowed maximum patch side-length and f_c being the upper frequency limit. For the membrane with $c_x = \sqrt{T_x/\rho_m t_m} \approx 95\ \text{m}/s$, $c_y \approx 27\ \text{m}/s$, the patch dimension in the axial and lateral directions is required to be smaller than $\Delta l_x = 0.12\text{m}$ and $\Delta l_y = 0.034\text{m}$, respectively. The interface 3 with a surface area of $0.85 \times 0.17\text{m}$ is therefore divided into $10 \times 10 = 100$ patches, satisfying the above convergence criteria.

In Fig. 4(a), the system TL calculated using the proposed formulation in Section 2 is plotted, where an excellent agreement can be seen between the present result and the reference one [19]. The membrane responses, i.e., the real part of the membrane velocity at the three distinct peaks located at P1 = 0.0625, P2 = 0.085, P3 = 0.117 are given in Fig. 4(b)–(d), which also in agreement with the modal analyses presented in Ref. [16]. Defining an acoustic stop-band with a criterion value of 10 dB, it is noted that the stop-band provided by such silencer is typically in the low frequency range, roughly from 120 Hz to 180 Hz in dimensional frequencies.

For the acoustic resonator configuration shown in Fig. 1(c), experiments were conducted to validate the numerical prediction using the proposed formulation. A piece of dielectric elastomer (VHB4910) manufactured by 3 M was stretched and attached to the neck area between the duct and side-branch. The system parameters were chosen as $h_d = h_{sc} = L_y = 0.16\text{m}$, $L_x = 0.135\text{m}$, $\rho_{\text{m}} = 1000\ \text{kg}/m^3$, $t_m^0 = 1\text{mm}$, and two membrane pre-stretch ratios $\delta = 4$ and $\delta = 3$ were tested in two separate experiments. The experimental test-rigs based on the well-established four-microphone, two-load method [14,22] were used for TL measurement. A loudspeaker driven by white noise signal in the interested frequency

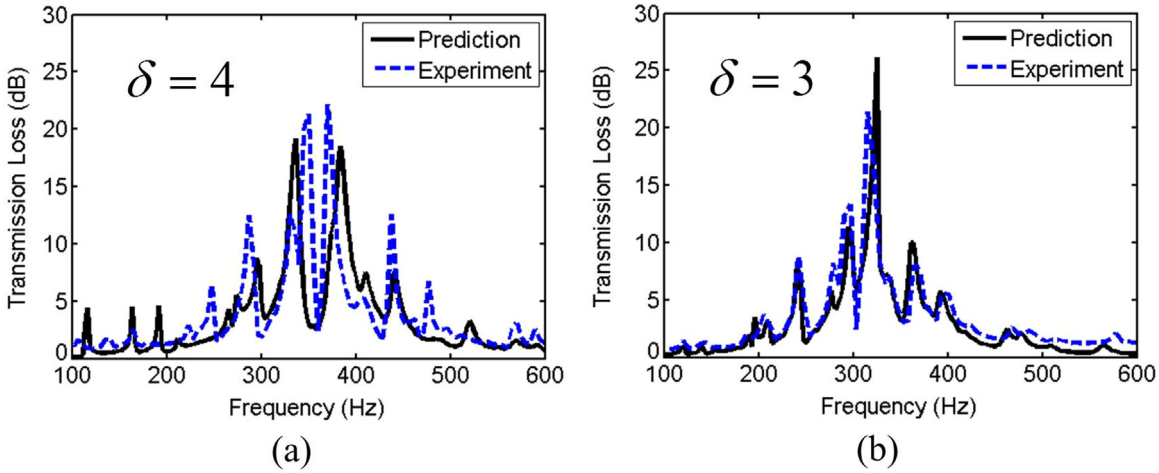

Fig. 5. Experimental validation of the numerical predictions using the proposed approach, for two pre-stretched membranes with (a) $\delta = 4$; (b) $\delta = 3$.

range is implemented as the sound source at the duct inlet. Two pairs of PCB microphones are used at the duct upstream and downstream to measure the sound pressures for determining the TL of the resonator.

For the first case with $\delta = 4$, the thickness of the stretched membrane calculated by Eq. (15) is $t_m = 0.0625$mm. In order to determine the tensile force T applied to the membrane, a structural FEM model using commercial software Abaqus was developed to calculate the membrane inner stress. By assuming a Neo-Hookean hyperplastic material model with a shear modulus of 25 kPa [8], simulation yields an inner stress of $\sigma = 398$kPa for the pre-stretched membrane, and the distributed tensile force is $T = \sigma t_m = 25$ N/m. For an interested frequency up to 600 Hz, $c_m = \sqrt{T/\rho_m t_m} = 20$ m/s requires the patch size to be smaller than $\Delta l = 0.017$m. The DE membrane at interface 3 is then divided into $N_x \times N_y = 12 \times 10$ patches. In the calculation, the membrane damping loss factor η_m is set as 0.03. In terms of computational time, the proposed model takes only about 20 s to run the simulation for a frequency range from 100 Hz to 600 Hz with a step-size of 3 Hz, benefiting from the averaged patch nature and the modal based subsystem treatments.

In Fig. 5(a), the predicted and measured TLs for $\delta = 4$ are compared. It can be seen that the prediction agrees reasonably well with experimental curve in terms of general tendency as well as peak locations, thus validating the proposed model. The noticeable discrepancies may come from the imperfections when fabricating the DE sample and also the experimental errors. A similar comparison is conducted for another case with pre-stretch ratio $\delta = 3$. The structural FEM analysis for determining the membrane inner stress gives $\sigma = 220.5$kPa, and the tensile force $T = 24.4$ N/m. As shown in Fig. 5(b), a very good agreement between the prediction and experiment is again observed. It can be seen from Fig. 5 that the present resonator provides sound attenuation bands typically in the medium frequency range from 250 to 450 Hz. The produced TL peaks are strong but in relatively narrow bandwidth.

Using the proposed approach, the reflection and absorption coefficients calculated via Eq. (13) are used to analyze the attenuation mechanism of the resonator. For both resonators with $\delta = 4$ and $\delta = 3$, the theoretical R and α curves versus frequency are plotted in Fig. 6. It can be seen that the attention is mainly attributed to the sound reflection mechanism, as a result of the induced membrane vibration and its radiation back to the duct upstream. The absorption mechanism is also significant at the system resonances, which plays an important role in determining the relative level and bandwidth of the TL peaks. It is also noted that the effective TL peaks of the resonator are generated by the structure-acoustic coupling through higher-order membrane modes. For example when $\delta = 4$, the natural frequency of the fundamental membrane mode, calculated by Eq. (22) with $n_x = n_y = 1$, is located at $f_{(1,1)} = 97$ Hz. This also means that the effective TL region at around 350 Hz in Fig. 5(a) has embraced at least the combined behavior of the first 17 structural modes. Thus, conducting a detailed modal analysis as previously done by Huang [16] is not pursued in this study.

4. Effect of applying voltage control

The effect of introducing voltage control to the DE membrane, in seeking a possible tuning of the resonator TL, is investigated in this section. As expressed in Eq. (17), when the electrodes on both sides of the membrane is subjected to an electrical potential, the Maxwell stress squeezes the membrane and enlarges its surface, causing a decrease in the membrane inner stress σ. Here, this relation was quantitatively determined by using the developed Abaqus FEM program. The variations of the membrane stress σ with applied voltage ranging from 0 kV to 6 kV are tabulated in Fig. 7, for both pre-stretch conditions with $\delta = 4$ and $\delta = 3$. In utilizing these FEM data as the input to the membrane tensile force in Eq. (18), a linear regression analysis was performed to find the relation between σ and V, which gives:

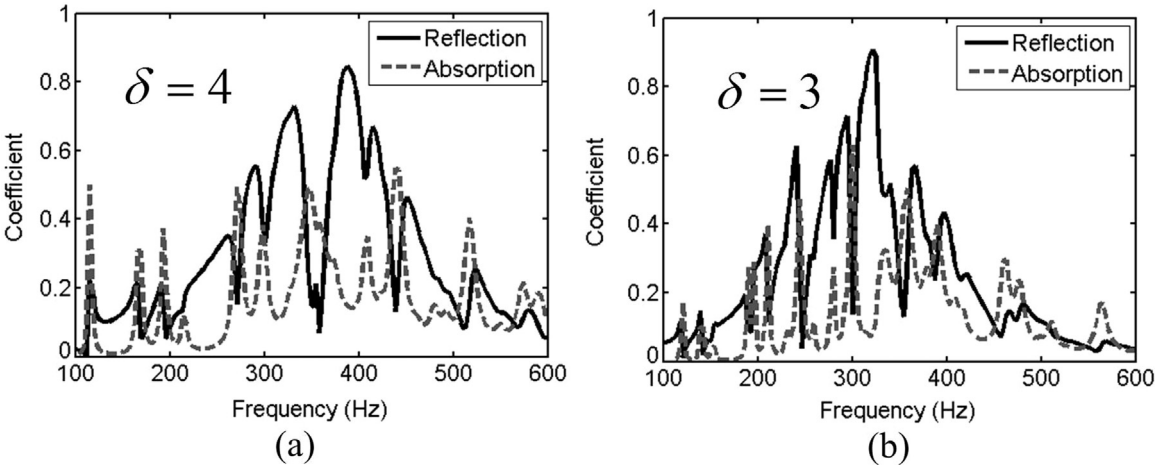

Fig. 6. Reflection and absorption coefficients of the resonator calculated using the proposed approach: (a) $\delta = 4$; (b) $\delta = 3$.

$$\sigma_{\delta=4} = 398 - 9.2V^2$$
$$\sigma_{\delta=3} = 220 - 2.6V^2 \tag{36}$$

Note that the units for σ and V used in the above relation are kilopascal (kPa) and kilovolt (kV), respectively. In Fig. 7, an excellent agreement between the FEM data and regression curve can be observed.

Embedding Eq. (36) into the proposed model, the silencing performance of the resonator with an increasing voltage applied to the DE membrane is studied. The membrane damping loss factor η_m is reduced to 0.01 to better identify the TL peak locations. For $\delta = 4$, the TLs corresponding to three different voltage levels are presented in Fig. 8. The benchmark case with $V = 0$kV, $\sigma = 398.1$kPa shows acoustic stop-bands in the vicinity of the four peaks located at 331 Hz, 385 Hz, 403 Hz and 430 Hz, respectively. These peaks are shifted to 316 Hz, 367 Hz, 385 Hz and 412 Hz when the applied voltage is raised to 2 kV with $\sigma = 360.9$kPa. To explain this, it can be seen from Eq. (22) that when the dimension of the membrane is fixed, the natural frequencies of the *in-vacuo* structural modes are proportional to $c_m = \sqrt{\sigma/\rho_m}$. This indicates that a factor of $\gamma_{0\to2} = \sqrt{\sigma_2/\sigma_0} = \sqrt{360.9/398.1} = 0.952$ may be suggested to correct the frequency shift when increasing voltage from 0 kV to 2 kV, assuming that the structural modes dominate the TL positions. In Table1, these TL peak positions and the corrected values by using $\gamma_{0\to2}$ are tabulated, which are in good agreement. When the applied voltage is adjusted to 4 kV, the correction factor yields $\gamma_{0\to4} = \sqrt{\sigma_4/\sigma_0} = \sqrt{250.5/398.1} = 0.794$, suggesting that the four peaks may be relocated to 263 Hz, 303 Hz, 320 Hz and 342 Hz. From the TL plot with $V = 4$ kV in Fig. 8, the first, third and fourth TL peaks are shifted down to 265 Hz, 327 Hz and 350 Hz, which can be well accounted by $\gamma_{0\to4}$. The second peak appears at the expected location but with a lower TL level. Overall speaking, the TL tuning mechanism is seen to be controlled by the membrane resonance shift which is triggered by the change in its inner stress. The effect of voltage control can be estimated by the proposed correction formula.

The above analyses show the potential of using the proposed resonator for adaptive-passive noise control. One example may be the control of fan noise, which is usually restricted to a narrow frequency band and dwells in the frequency range from 100 Hz to 500 Hz [20]. The tuning ability and the achievable tuning range of the proposed resonator are further investigated through parametric studies. With $\delta = 4$, Fig. 9 illustrates the TL variations against continuous voltage change, in

Voltage (kV)	Stress (kPa): δ=4	Stress (kPa): δ=3
0	398.1	220.5
1	388.6	216.5
2	360.9	210.5
3	314.9	199.6
4	250.5	180.9
5	168.8	151.5
6	66.6	124.3

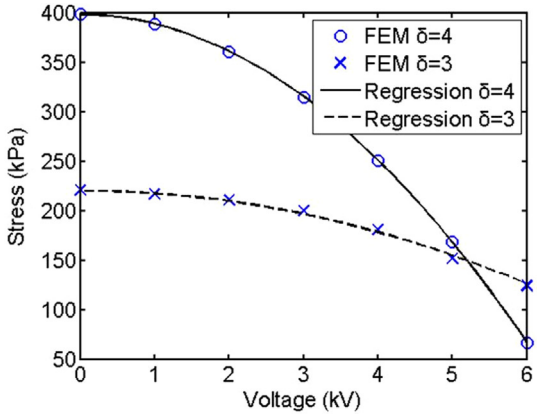

Fig. 7. Variation of membrane stress σ with altering applied voltage V.

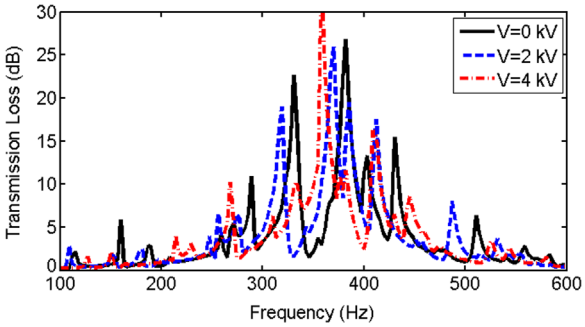

Fig. 8. TLs of the resonator with increasing applied voltage from 0 kV to 4 kV, pre-stretch ratio $\delta = 4$.

Table 1
Increasing the voltage control from 0 kV to 2 kV and 4 kV, the shifting of TL peak positions and the corrected values using $\gamma_{0\to2}$ and $\gamma_{0\to4}$.

Voltage	0 kV	2 kV (by $\gamma_{0\to2}$)	2 kV	4 kV (by $\gamma_{0\to4}$)	4 kV
1st peak	331 Hz	315 Hz	316 Hz	263 Hz	265 Hz
2nd peak	385 Hz	367 Hz	367 Hz	303 Hz	310 Hz
3rd peak	403 Hz	384 Hz	385 Hz	320 Hz	327 Hz
4th peak	430 Hz	410 Hz	412 Hz	342 Hz	350 Hz

which a total of 50 voltages are linearly sampled from 0 kV to 6 kV. Beyond 6 kV, the DE membrane may fail due to electric breakdown. The gradual shifting behavior of the TL peaks shows the appealing feature of the proposed device in that it can provide a controllable and roughly predictable attenuation performance. The achievable tuning range, as an important constraint to be input to the control algorithm, is illustrated in Fig. 10, showing that the major TL peaks fall into the frequency range between 300 Hz and 450 Hz. Similar analyses for $\delta = 3$ are presented in Figs. 11 and 12, where the gradual TL shifting is again clearly observed. The possible tuning range for acoustic stop-bands is primarily changed to 250–400 Hz. Within such region, adaptive algorithm can be developed to adjust the applied voltage and to tune the system TL, so that the resonator can catch some of the discrete noise peaks at the fundamental frequencies and their harmonics. Having said that, the proposed device cannot address the attenuation of broadband noise based on its current geometry and configuration, as a major limitation. The material and geometrical effects on the TL response also need to be clarified before its actual implementation.

Finally, it should be mentioned that the results presented herein are based on linear assumption of structure-acoustic interactions, where the mass effects of the electrodes, possible internal flow and non-linear membrane deformation are neglected. The proposed modelling framework can be extended to include multiple resonators, being cascaded into a duct silencer [26] or periodically arranged into an acoustic metasurface [27]. The extension should be straightforward due to the modular and sub-structuring nature of the method. With various parameters involved, resonators can be individually tuned to meet different specifications to achieve a desired overall acoustic performance.

5. Conclusions

The acoustic property of a resonator comprising a side-branch cavity covered by an electro-active membrane has been

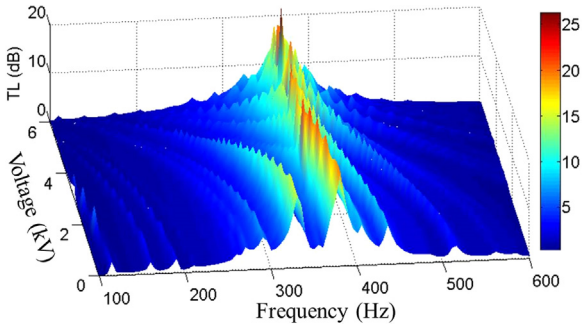

Fig. 9. TL variations against continuous voltage change, pre-stretch ratio $\delta = 4$.

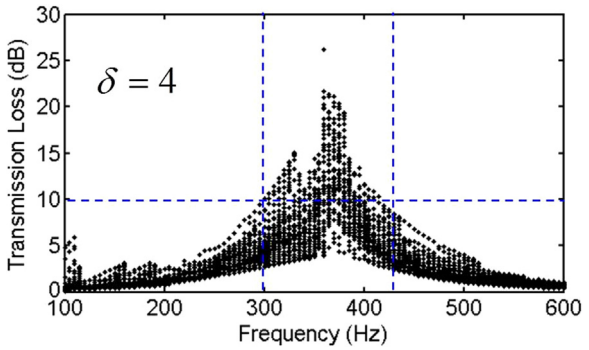

Fig. 10. The achievable tuning frequency range of the acoustic stop-bands, $\delta = 4$.

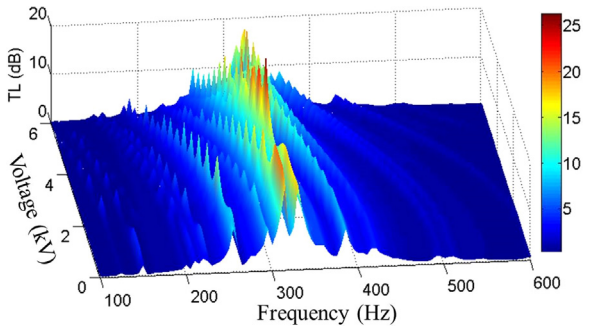

Fig. 11. TL variations against continuous voltage change, pre-stretch ratio $\delta = 3$.

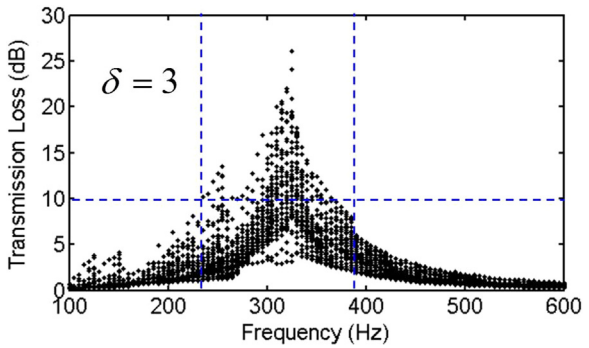

Fig. 12. The achievable tuning frequency range of the acoustic stop-bands, $\delta = 3$.

investigated. A pre-stretched DE film with electrodes coated on both surfaces for voltage control was considered. The resonator provides sound attenuation in the medium frequency range mainly through membrane vibration and its radiation back to the duct upstream. The transmitted sound power to the duct downstream is therefore reduced due to destructive acoustic interference.

A fully coupled, three-dimensional vibroacoustic model was developed. The coupling framework was enabled by a sub-structuring treatment based on the transfer function relations determined at the interfaces. Subsystems including the DE membrane, duct and acoustic cavity were formulated using a modal expansion approach. Experimental validations were conducted, showing a generally good agreement between the simulation and measurement.

It has been shown that the TL response of the system can be controlled through altering the control voltage applied to the DE membrane. Physically, the applied voltage causes an elongation in the membrane surface and a decrease in its inner stress, which subsequently changes the *in-vacuo* modes of the membrane and the structure-acoustic coupling response. The shifting mechanism of TL peaks was clearly observed with the help of numerical simulations, and a correction factor was suggested for the estimation of this frequency shift.

In views of possible use of the proposed resonator as an adaptive-passive device for noise control, the tunable and achievable frequency range of the device was investigated. Under the current system parameters, a DE membrane with a pre-stretch ratio $\delta = 4$ can tune the effective resonator TL in the region of 300–450 Hz, by adjusting the voltage up to 6 kV. With a lower pre-stretch ratio of $\delta = 3$, the frequency range can be lower down to 250–400 Hz. Through the presented

results and analyses, the proposed resonator shows considerable potential for applications such as silencer or absorber design for acoustic ducts or ventilation systems.

Acknowledgements

This material is based on research/work supported by the Singapore Ministry of National Development and National Research Foundation under L2 NIC award No. L2NICCFP1-2013-9.

References

[1] D.A. Bies, C.H. Hansen, *Engineering Noise Control: Theory and Practice*, CRC Press, United States, 2009.
[2] D. Zhao, A.S. Morgans, Tuned passive control of combustion instabilities using multiple Helmholtz resonators, *J. Sound Vib.* 320 (2009) 744–757.
[3] K. Nagaya, Y. Hano, A. Suda, Silencer consisting of two-stage Helmholtz resonator with auto-tuning control, *J. Acoust. Soc. Am.* 110 (2001) 289–295.
[4] C.Q. Howard, R.A. Craig, An adaptive quarter-wave tube that uses the sliding-Goertzel algorithm for estimation of phase, *Appl. Acoust.* 78 (2014) 92–97.
[5] T.L. Huang, M.N. Ichchou, O.A. Bareille, M. Collet, M. Ouisse, Multi-modal wave propagation in smart structures with shunted piezoelectric patches, *Comput. Mech.* 52 (2013) 721–739.
[6] F. Carpi, D. De Rossi, R. Kornbluh, R.E. Pelrine, P. Sommer-Larsen, *Dielectric Elastomers as Electromechanical Transducers: Fundamentals, Materials, Devices, Models and Applications of an Emerging Electroactive Polymer Technology*, Elsevier Science, United Kindom, 2011.
[7] Z. Suo, Theory of dielectric elastomers, *Acta Mech. Solida Sin.* 23 (2010) 549–578.
[8] W. Lai, *Characteristics of Dielectric Elastomers and Fabrication of Dielectric Elastomer Actuators for Artificial Muscle Applications* (Master thesis), Iowa State University, United States, 2011, 15–16.
[9] K. Hochradel, S.J. Rupitsch, A. Sutor, R. Lerch, D.K. Vu, P. Steinmann, Dynamic performance of dielectric elastomers utilized as acoustic actuators, *Appl. Phys. A* 107 (2012) 531–538.
[10] P. Dubois, S. Rosset, M. Niklaus, M. Dadras, H. Shea, Voltage control of the resonance frequency of dielectric electroactive polymer (DEAP) membranes, *J. Microelectromechanical Syst.* 17 (2008) 1072–1081.
[11] J. Zhu, S. Cai, Z. Suo, Resonant behavior of a membrane of a dielectric elastomer, *Int. J. Solids Struct.* 47 (2010) 3254–3262.
[12] R. Heydt, R. Kornbluh, J. Eckerle, R. Pelrine, Sound radiation properties of dielectric elastomer electroactive polymer loudspeakers, in: Smart Structures and Materials, International Society for Optics and Photonics, 2006, pp. 61681M-61681M-61688.
[13] R. Heydt, R. Pelrine, J. Joseph, J. Eckerle, R. Kornbluh, Acoustical performance of an electrostrictive polymer film loudspeaker, *J. Acoust. Soc. Am.* 107 (2000) 833–839.
[14] Z. Lu, H. Godaba, Y. Cui, C.C. Foo, M. Debiasi, J. Zhu, An electronically tunable duct silencer using dielectric elastomer actuators, *J. Acoust. Soc. Am.* 138 (2015) EL236–EL241.
[15] L. Huang, A theoretical study of duct noise control by flexible panels, *J. Acoust. Soc. Am.* 106 (1999) 1801–1809.
[16] L. Huang, Modal analysis of a drumlike silencer, *J. Acoust. Soc. Am.* 112 (2002) 2014–2025.
[17] L. Huang, Parametric study of a drum-like silencer, *J. Sound Vib.* 269 (2004) 467–488.
[18] L. Huang, Broadband sound reflection by plates covering side-branch cavities in a duct, *J. Acoust. Soc. Am.* 119 (2006) 2628–2638.
[19] L. Huang, Y.S. Choy, Vibroacoustics of three-dimensional drum silencer, *J. Acoust. Soc. Am.* 118 (2005) 2313–2320.
[20] J.B. Lawrie, I.M. Guled, On tuning a reactive silencer by varying the position of an internal membrane, *J. Acoust. Soc. Am.* 120 (2006) 780–790.
[21] Y.S. Choy, L. Huang, Effect of flow on the drumlike silencer, *J. Acoust. Soc. Am.* 118 (2005) 3077–3085.
[22] X. Yu, L. Cheng, Duct noise attenuation using reactive silencer with various internal configurations, *J. Sound Vib.* 335 (2015) 229–244.
[23] X. Yu, L. Cheng, X. You, Hybrid silencers with micro-perforated panels and internal partitions, *J. Acoust. Soc. Am.* 137 (2015) 951–962.
[24] J.-D. Chazot, J.-L. Guyader, Prediction of transmission loss of double panels with a patch-mobility method, *J. Acoust. Soc. Am.* 121 (2007) 267–278.
[25] M. Ouisse, L. Maxit, C. Cacciolati, J.-L. Guyader, Patch transfer functions as a tool to couple linear acoustic problems, *J. Vib. Acoust.* 127 (2004) 458–466.
[26] X. Yu, Y. Tong, J. Pan, L. Cheng, Sub-chamber optimization for silencer design, *J. Sound Vib.* 351 (2015) 57–67.
[27] G. Ma, M. Yang, S. Xiao, Z. Yang, P. Sheng, Acoustic metasurface with hybrid resonances, *Nat. Mater.* 13 (2014) 873–878.